J Solid State Electrochem (2009) 13:333–340
DOI 10.1007/s10008-008-0560-0

ORIGINAL PAPER

A facile approach to the preparation of loose-packed $Ni(OH)_2$ nanoflake materials for electrochemical capacitors

Jun-Wei Lang · Ling-Bin Kong · Wei-Jin Wu · Min Liu · Yong-Chun Luo · Long Kang

Received: 24 January 2008 / Accepted: 6 April 2008 / Published online: 6 May 2008

Abstract Loose-packed nickel hydroxides were successfully synthesized by a facile chemical precipitation method. Structure characterizations indicate that a nanoflake structure with low crystallinity for the nickel hydroxide samples was obtained. Electrochemical studies were carried out using cyclic voltammetry, chronopotentiometry technology, and alternating current impedance spectroscopy, respectively. A maximum specific capacitance of 2,055F/g could be achieved in 2M aqueous KOH with the potential range of 0 to 0.4V (vs. the saturated calomel electrode) in a half-cell setup configuration for the nanoflake $Ni(OH)_2$ electrode, suggesting its potential application in the electrode material for electrochemical capacitors. Furthermore, the effect of annealing temperatures on the electrochemical capacitance characteristics has also been systemically explored.

Keywords Electrochemical capacitors · Nickel hydroxide · Specific capacitance · Nanoflakes

Introduction

In recent years, the growing interest in the use of electrochemical systems under conditions in which the electrical power demand is highly time dependent and growing environmental concerns and increasing depletion of fossil fuels have created interest in alternative energy technologies [1–2].

Electrochemical capacitors, which combine the advantages of the high power of dielectric capacitors and the high specific energy of rechargeable batteries, have played an increasingly important role in power source applications such as hybrid electric vehicles and short-term power sources for mobile electronic devices [3–5]. Many charge storage mechanisms have been proposed for electrochemical capacitors, most notably double-layer capacitance arising from the charge separation at the electrode/electrolyte interface and faradaic pseudocapacitance arising from fast, reversible electrosorption or redox processes occurring at or near the solid electrode surface [6]. The large specific capacitance of electrochemical capacitors is the result of one or a combination of these charge storage mechanisms. Moreover, the energy density of the relatively new pseudocapacitor devices that are based on faradaic processes has been reported many times because it has been recognized that the energy density based on pseudofaradaic processes is of many times greater than that of the traditional double-layer capacitors [7–9].

In particular, electrochemical capacitors based on hydrous ruthenium oxides exhibit much higher specific capacitance than conventional carbon materials and better electrochemical stability than electronically conducting polymer materials. However, the high material cost of $RuO_2 \times H_2O$ makes this material inadequate for commercial applications. Thus, developing alternative electrode materials with improved characteristics and performance is the next logical step. Since many transition metal oxides have been shown to be excellent electrode materials for electrochemical capacitors with their charge storage mechanisms based predominantly on pseudocapacitance [6], more and more attention has been paid to nickel oxides

J.-W. Lang · L.-B. Kong (✉) · W.-J. Wu · M. Liu · Y.-C. Luo · L. Kang
State Key Laboratory of Gansu Advanced Non-ferrous Metal Materials, Lanzhou University of Technology, Lanzhou 730050, People's Republic of China
e-mail: konglb@lut.cn

[10–12], cobalt oxides [13–16], or manganese oxides [6, 17–19], which show a good electronic conductivity, acceptable specific capacitance, and lower cost.

In recent years, nickel oxide, as one of the most important transition metal oxides, has received increasing attention due to its extensive applications, especially as a positive electrode-active material [20]. There are several methods used to prepare nickel oxides such as precipitation [21, 22], electrodeposition [23], and the sol–gel technique [24]. However, these processes largely lead to micrometer nickel oxides or aggregated nanostructural nickel oxides with a low specific capacitance. Since the capability of electrode materials is significantly influenced by its surface area and morphology, the electrode material with a high surface area and a uniform, ordered pore network of nanometer dimension would be expected to exhibit superior performance in an electrochemical capacitors system [10]. In this work, loose-packed $Ni(OH)_2$ materials with two morphologies (amorphous particles and nanoflake phase) were synthesized by a facile precipitation method with careful controlling of the preparative parameters such as the initial concentration of Ni^{2+}, the addition time, aging time, and processing temperature. This novel structure creates electrochemical accessibility of electrolyte OH^- ions to Ni $(OH)_2$ nanoflakes and a fast diffusion rate within the redox phase [25]. Electrochemical measurements were carried out in 2M aqueous KOH in a half-cell setup configuration at room temperature using cyclic voltammetry (CV), chronopotentiometry, and impedance spectroscopy, respectively. Electrochemical studies showed that the electrode has superior capacitive performance, and the maximum specific capacitance is up to 2,055F/g for a single-electrode system, which is the highest report of $Ni(OH)_2$ for electrochemical capacitors. In addition, the effect of annealing temperatures on the capacitance property of $Ni(OH)_2$ was also studied in detail.

Experimental

Material preparation

All of the chemicals were of analytical grade and used without further purification. $Ni(OH)_2$ materials was prepared by a facile-improved precipitation method. The first step was the confecting of the nickel chloride hydrate solution (Ni concentration = 1.0M) in a glass beaker, using a magnetic stir bar. The nickel chloride hydrate solution was slowly adjusted to pH9 by dropwise addition of 5wt% NH_4OH at a temperature of ~10 °C, controlling the addition time to more than 2h. The resulting suspension was stirred at this temperature for an additional 3h. Then, the solid was filtered, washed with a copious amount of distilled water, and dried at different temperatures in air for 6h.

Electrode preparation

The working electrodes were prepared according to the method reported in literature [26]. $Ni(OH)_2$ powder of 80wt% was mixed with 7.5wt% of acetylene black (>99.9%) and 7.5wt% of conducting graphite in an agate mortar until a homogeneous black powder was obtained. To this mixture, 5wt% of poly(tetrafluoroethylene) was added with a few drops of ethanol. After briefly allowing the solvent to evaporate, the resulting paste was pressed at 10MPa to a nickel gauze with a nickel wire for an electric connection. The electrode assembly was dried for 16h at 80 °C in air. Each electrode contained about 8mg of electroactive material and had a geometric surface area of about $1cm^2$.

Structure characterization

The obtained products were characterized by transmission electron microscope (TEM; JEOL, JEM-2010, Japan), field emission scanning electron microscope (SEM; JEOL, JSM-6701F), X-ray diffraction (XRD) measurements (Bruker, D8 Advance, Germany), thermogravimetric analysis (TGA; Netzsch, STA-449C, Germany), and nitrogen adsorption and desorption experiments (Micromeritics, ASAP 2010, USA). The surface area was calculated using the Brunauer–Emmett–Teller (BET) equation. Pore size distributions were calculated by the Barrett–Joyner–Halenda (BJH) method using the desorption branch of the isotherm.

Electrochemical tests

Electrochemical measurements were carried out using an electrochemical working station (CHI660C, Shanghai, China) in a half-cell setup configuration at room temperature. A platinum gauze electrode and a saturated calomel electrode (SCE) served as the counter electrode and the reference electrode, respectively. CV scans were recorded from −0.3 to 0.75V at different scan rates in 2M KOH aqueous solution, and charge–discharge cycle tests were carried out in the potential range of 0–0.4V in 2M KOH aqueous solution at different constant current densities. Electrochemical impedance spectroscopy measurements were performed under open circuit potential in an alternating current frequency range from 10,000 to 0.01Hz with an excitation signal of 5mV. All electrochemical experiments were carried out at 20 ± 1 °C.

Results and discussion

TGA was conducted for as-prepared $Ni(OH)_2$ materials in argon atmosphere to examine the conversion process during

calcinations. Shown in Fig. 1, the sample weight decreases slowly between 100 and 240 °C; this is expected to be due mainly to the removal of chemically adsorbed H_2O. A very obvious weight loss of 10.65% is present between 240 and 290 °C on the TGA curve, which is believed that the reaction of

$$Ni(OH)_2 \rightarrow NiO + H_2O \quad (1)$$

occurs in this region. With the increase in temperature to more than 290 °C, the TGA curve becomes flat, which indicates that no phase transformation occurs, and further heating could only make the structure of the products more crystalline, which is confirmed by the following XRD results.

Shown in Fig. 2 are the XRD patterns of the $Ni(OH)_2$ materials and the corresponding samples heated at different temperatures for 6h in air. No obvious peaks of β-nickel hydroxide have been observed in the XRD pattern of the as-prepared $Ni(OH)_2$ obtained at 100 °C, and it corresponds to the layered α-$Ni(OH)_2$ structure with low crystallinity. A conversion of nickel hydroxide to nickel oxide took place as the temperature increased from 100 to 250 °C. Being heated at 250 °C for 6h, almost all of the $Ni(OH)_2$ were converted to NiO with a less crystalline structure. The XRD patterns exhibit the characteristic peaks of rock salt NiO at 2θ = 37, 43, and 63°, which first appeared in the resultant materials at 220 °C [20, 27, 28]. This result is in agreement with that of the TGA.

The morphology of as-prepared $Ni(OH)_2$ is examined by SEM and TEM. Two morphologies (amorphous particles and nanoflakes) can be seen in Fig. 3a and b. It is noteworthy that the network-like structure (which consists of interconnected nanoflakes) shows anisotropic morphology characteristics and the formation of a loosely packed microstructure in the nanometer scale. The unique structure

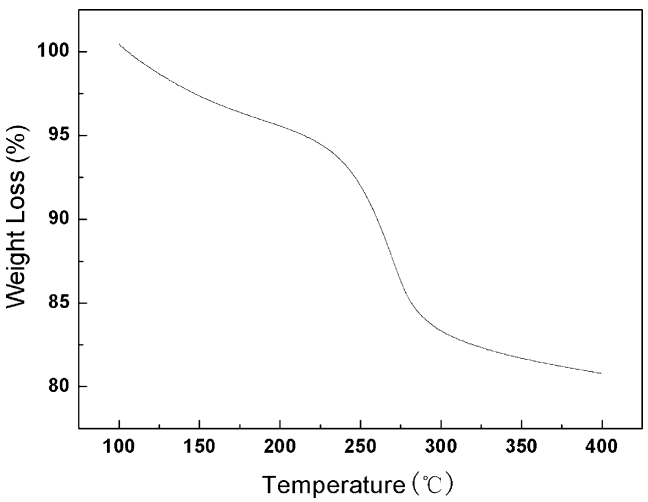

Fig. 1 TGA plots of as-prepared $Ni(OH)_2$

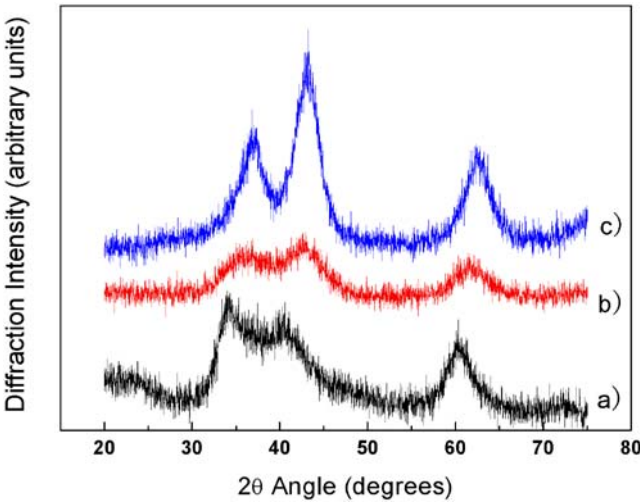

Fig. 2 XRD of as-prepared $Ni(OH)_2$ materials and corresponding samples heated at different temperatures for 6 h in air: **a** 100, **b** 220, and **c** 250 °C

plays a basic role in the morphology requirement for the electrochemical accessibility of electrolyte OH^- to $Ni(OH)_2$ active material and a fast diffusion rate within the redox phase. It is believed that the unique structure provided an important morphological foundation for the extraordinary high specific capacitances.

To understand the reason why the flake-like structure of the $Ni(OH)_2$ phase can be formed during the synthesis process, a formation mechanism from aggregation growth to surface growth in the solution can be summarized as follows: Shown in Fig. 4, the initial precipitations provide numerous $Ni(OH)_2$ nucleation centers. Because of the anisotropy of α-$Ni(OH)_2$ crystals, the growing point of each crystal is located at certain directions, so nanoflakes will be formed. These α-$Ni(OH)_2$ nanoflakes consist lots of interbedded water, which are distributed at certain directions. When the sizes of these flakes become larger, their tendency to aggregate is increased. As a result, the microsphere of nanoflake aggregation will be formed due to the strong hydrogen bond of H_2O. With the reaction going on, new $Ni(OH)_2$ nanoflakes will grow up around the nucleation centers at the surface of the microsphere. The surface growth leads to the continuous increase in size and density of the microsphere to form a network structure [29].

Surface area and pore size distribution analysis of these materials were conducted using N_2 adsorption and desorption experiments. As seen from Fig. 5, the profile of the hysteresis loop indicates an adsorption–desorption characteristic of the porous materials. The as-prepared $Ni(OH)_2$ possesses a narrow mesoporous distribution at around 4–10nm and has a surface area of about 11m^2/g. The materials did not have a very high specific surface area and porous volume due to the presence of a large amount of amorphous particles. Further study will be carried out to analyze the

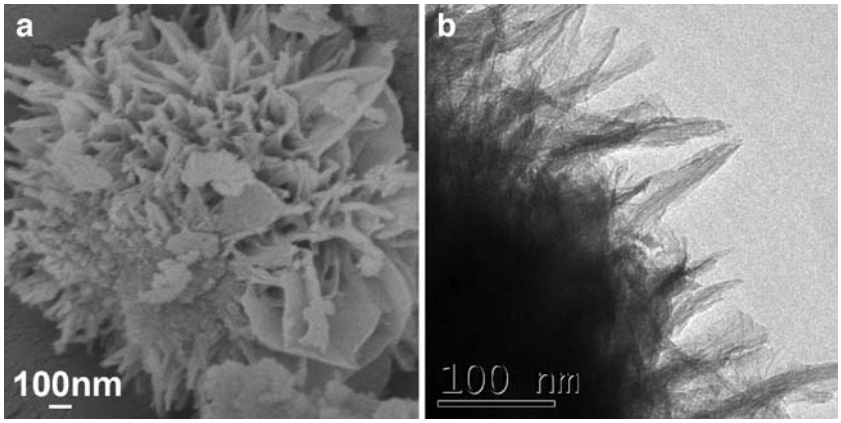

Fig. 3 **a** SEM image of as-prepared $Ni(OH)_2$ obtained at 100 °C; **b** TEM image of as-prepared $Ni(OH)_2$ obtained at 100 °C

effect of PH value and the concentration of ammonia on the aggregate structure of $Ni(OH)_2$ particles, for only the interconnected nanoflake structure leads to a high surface-specific area and porous volume, which provide the structural foundation for the high specific capacitance.

CV and chronopotentiometry measurements have been used to evaluate the electrochemical properties and quantify the specific capacitance of the as-prepared $Ni(OH)_2$ electrodes. Figure 6a shows the CV curves of the $Ni(OH)_2$ electrode. The shape of the CV reveals that the capacitance characteristic is very distinguished from that of electric double-layer capacitance in which the shape is normally close to an ideal rectangular shape. These indicate that the capacity mainly results from the pseudocapacitive capacitance, which is based on a redox mechanism. It is well accepted that the surface faradaic reactions will proceed according to the following reaction [25].

$$Ni(OH)_2 + OH^- \leftrightarrow NiOOH + H_2O + e^- \quad (2)$$

The two strong redox reaction peaks are responsible for the pseudocapacitance. The anodic peak P1 is due to the oxidation of $Ni(OH)_2$ to NiOOH, and the cathodic peak P2 is for the reverse process. It should be noted that with the sweep rate increased, the shape of the CV changed, the anodic peak potential and cathodic peak potential shift in the more anodic and more cathodic direction, and the capacitance, inevitably, decreased, which is in agreement with the result of the chronopotentiometry measurement.

Figure 6b shows the discharging curves of the $Ni(OH)_2$ electrode obtained in the potential range of 0–0.4V in 2M KOH at various current rates (5, 10, 20, and 30mA). The shape of the discharge curves does not show the characteristic of the pure double-layer capacitor but mainly pseudocapacitance, which is in agreement with the result of the CV curves. The curves obviously display two variation range: A linear variation of the time dependence of the potential (below about 0.15V) indicates the double-layer capacitance behavior, which is caused by the charge

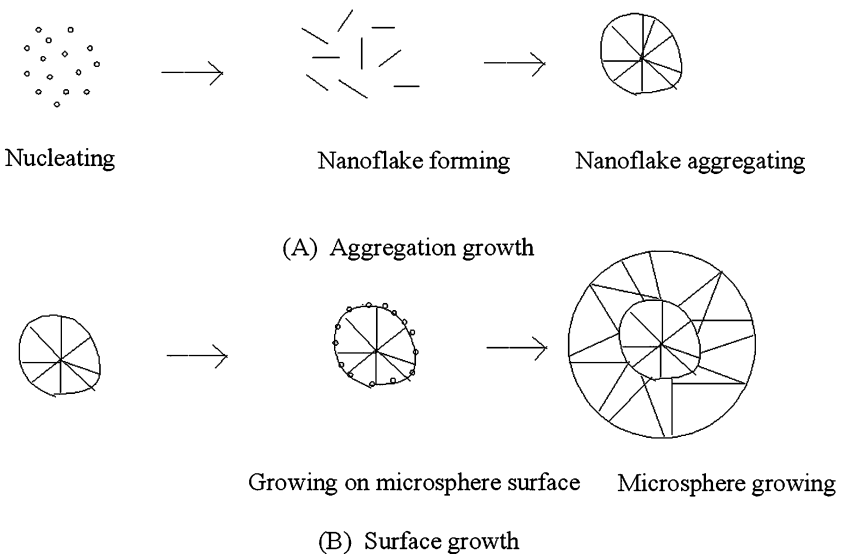

Fig. 4 Schematic formation mechanism of the as-prepared $Ni(OH)_2$

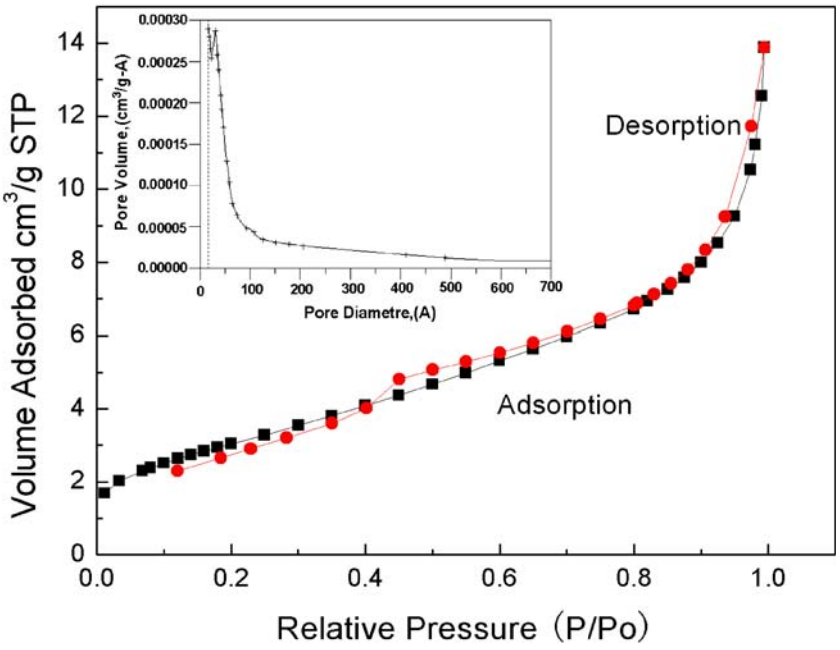

Fig. 5 The N_2 adsorption–desorption isotherm of as-prepared $Ni(OH)_2$ obtained at 100 °C. The *inset* shows BJH pore size distributions

separation taking place between the electrode and electrolyte interface, and a slope variation of the time dependence of the potential (from 0.4 to 0.15V) indicates a typical pseudocapacitance behavior, which resulted from the electrochemical adsorption/desorption or redox reaction at an interface between electrode and electrolyte [10]. The corresponding specific capacitance was calculated from $C = I/[(dE/dt) \times m] \approx I/[(\Delta E/\Delta t) \times m]$, where I is the constant discharging current, dE/dt indicates the slope of the discharge plot of the discharging curves, and m is the mass of the corresponding electrode materials measured. In this way, the specific capacitance of the $Ni(OH)_2$ materials at 5, 10, 20, and 30mA were 2,055, 1,907, 1,645, and 1,486F/g. It is obvious to note that the highest specific capacitance for $Ni(OH)_2$ phase measured at 5mA is close to the theoretical value (2,602.5F/g) assuming nearly all Ni $(OH)_2$ in the bulk is electrochemically accessible and contributes to capacitance [2].

As the discharge current increases, the large voltage drop produces, and finally, the capacitance decreases. This phenomenon may be explained by referring OH^- ions diffusion processes during the charging/discharging for the electrode. When the electrode at high sweep rates corresponds to high current density, massive OH^- ions are required to intercalate swiftly at the interface of electrode/electrolyte; however, a relatively low concentration of OH^- ions could not meet this demand, and the processes would be controlled by the ion diffusion [30]. However, the discharge capacitance at 10mA is 92.7% of that discharged at 5mA, so the excellent rate capability of the sample makes it attractive particularly for a practical application.

Additionally, once the oxide phase is formed, further heat treatment at a higher temperature may cause the increase in crystal size and, accordingly, the decrease in specific surface area and, also possibly, its reactivity for surface chemical process, thereby leading to a decreased capacitance [9]. Just as in the case of RuO_2, its amorphous phase exhibited far greater specific capacitance than the crystalline counterpart [31]. Figure 7 shows the effect of annealing temperature on the capacitive properties of the Ni $(OH)_2$ electrodes. With increasing annealing temperature, the decline tendency of the specific capacitance is similar and irrelevant to different discharge currents. Although the samples obtained at 100 and 150 °C have almost the same specific capacitance at a discharging current density of 5mA/cm^2, the sample obtained at 100 °C has a better rate capability than that of obtained at 150 °C.

Figure 8 shows the complex plane plots of the impedance of the $Ni(OH)_2$ electrodes prepared at different temperatures (at 0.27V, near open circuit potential). The complex plane impedance plots for each sample can be divided into the high-frequency component and the low-frequency component. A distinct knee in the frequency can be observed in curves of Fig. 8. From the point intersecting with the real axis in the range of high frequency, the internal resistances (which is equal to R_b) of the electrode material is in the order of NiO (1.25Ω) < $Ni(OH)_2$ (1.6Ω). It includes the total resistances of the ionic resistance of the electrolyte, the intrinsic resistance of active materials, and the contact resistance at the active material/current collector interface. The semicircle in the high-frequency range associates with the surface properties of the porous

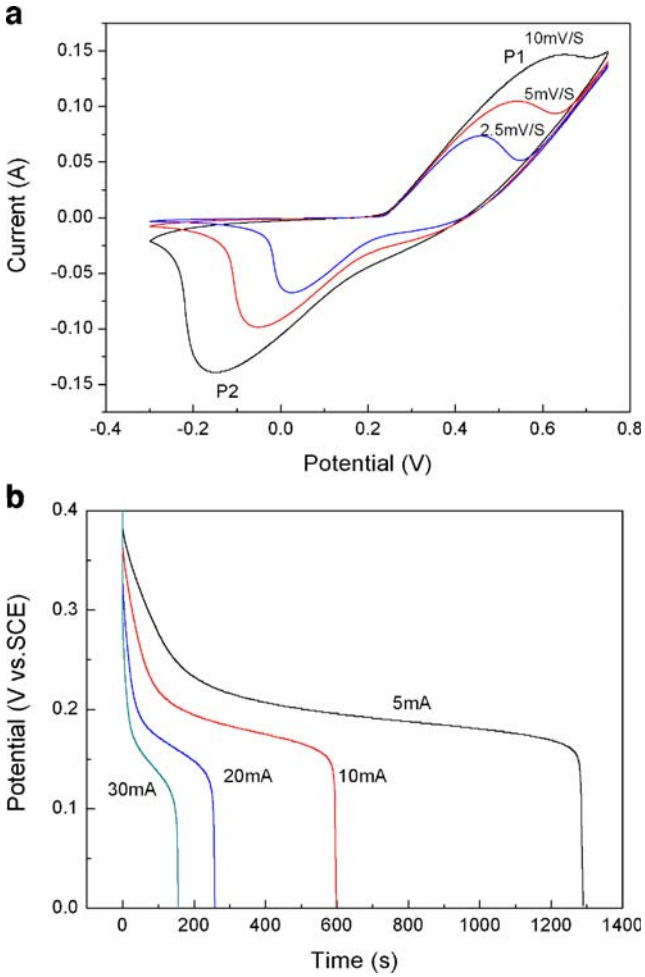

Fig. 6 Electrochemical properties of $Ni(OH)_2$ in the 2 M KOH solution: **a** CV curves at different scan rates within a potential window of −0.3–0.75 V vs. SCE; **b** discharging curves in the potential range from 0.4 to 0 V at different discharging currents. The working electrode is 1 cm^2 containing about 8 mg $Ni(OH)_2$

electrode, which corresponds to the faradic charge transfer resistance (R_{ct}). It can be seen that the samples both have a small faradic charge transfer resistance, and the impedance of the NiO electrode is smaller than that of the $Ni(OH)_2$ electrode. This can be explained that with the increase in the heat treatment temperature, the increase in the pore diameter can enhance the diffusivity of the electrolyte irons in the pores. However, the overall decreasing equivalent series resistance conductive to increase capacitance cannot compensate for the loss of the capacitance in the experimental energy density due to the decreased specific surface area resulting from the increased particle diameter [15]. At the lower frequencies, a straight sloping line represents the diffusive resistance (Warburg impendence) of the electrolyte in electrode pores and the proton diffusion in host materials. The phase angles for impedance plots of both electrodes were observed to be higher than 45° in the low frequencies clearly. These findings suggest that both electrodes are not controlled by the diffusion process. These may be attributed to the ordered mesoporous distribution, which can facilitate ionic motion [32, 33].

The long-term electrochemical stability of the $Ni(OH)_2$ in the 2M KOH electrolyte has been examined by chronopotentiometry. As shown in Fig. 9, the cycling stability was tested over 1,500 cycles. It exhibited a loss of 54.2% in capacitance during the first 400 cycles, which indicates that the repetitive charge–discharge cycles do induce a noticeable degradation of the microstructure. After this stage, a comparatively slow loss was observed, and the value of the 1,500th cycle still remained at 65.25% of the 400th cycle. The nickel hydroxide crystallizes in two

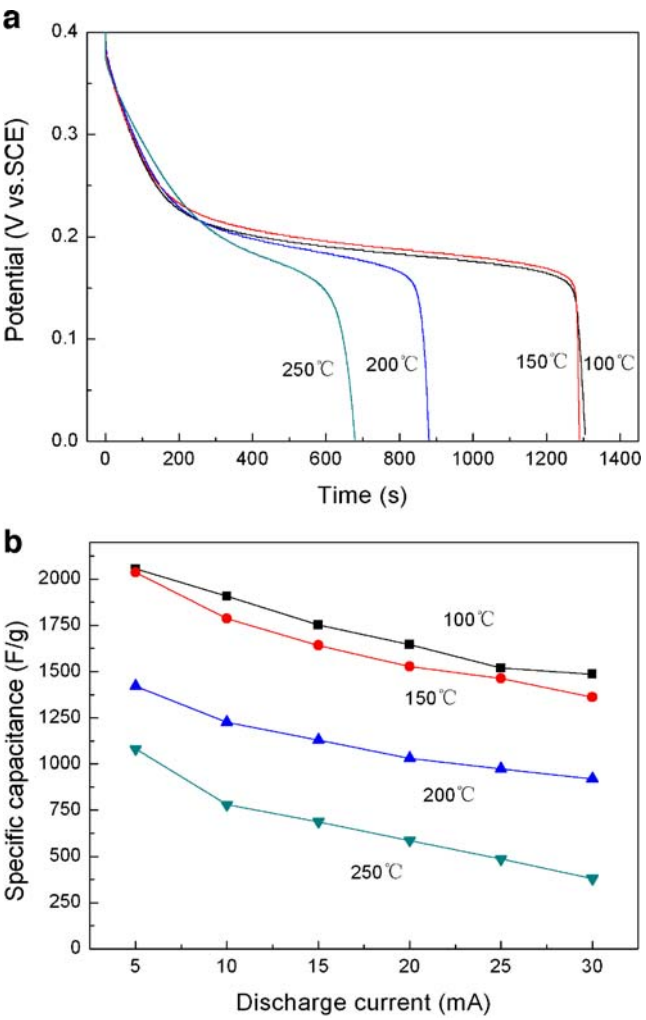

Fig. 7 Electrochemical properties of $Ni(OH)_2$ materials and corresponding samples heated at different temperatures in the 2 M KOH solution: **a** discharging curves in the potential range from 0.4 to 0 V at the discharging current of 5 mA; **b** the specific capacitance as a function of discharge currents. The working electrode is 1 cm^2 containing about 8 mg $Ni(OH)_2$ or the corresponding samples

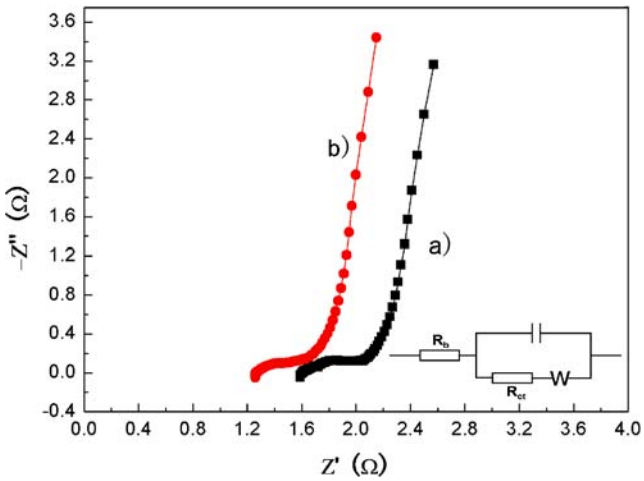

Fig. 8 Complex plane impedance plots of the $Ni(OH)_2$ electrodes prepared at different heat treatment temperatures: a 100 and b 250 °C (0.27 V vs. SCE; electrolyte: 2 M KOH). The *inset* is the equivalent circuit

polymorphic modifications known as α and β. Consequently, the reversible reactions of nickel hydroxide involve two redox couples namely, the α-$Ni(OH)_2$/γ-NiOOH and the β-$Ni(OH)_2$/β-NiOOH. α-$Ni(OH)_2$ can be cycled to the γ-NiOOH phase reversibly without any mechanical deformation. Besides, a larger number of electrons are exchanged per nickel atom during the α↔γ phase transformation, since the oxidation state of nickel in γ-NiOOH is close to 3.5; a higher theoretical capacity for the nickel-positive electrode comprising α-$Ni(OH)_2$ is envisaged in relation to a β-$Ni(OH)_2$ electrode. However, α -Ni $(OH)_2$ happens to be unstable in an alkaline medium and transforms to β-$Ni(OH)_2$, and the α/γ couple is rapidly aged to the β/β couple [28, 34]. Therefore, the capacitance fading may originate from the slow transformation of α-Ni $(OH)_2$ to β-$Ni(OH)_2$. We can further produce a stabilized α-$Ni(OH)_2$ as an electrode material since the presence of dissolved cations such as Al and Zn in an alkaline electrolyte can suppresses the α→β nickel hydroxide transformation [28]. Work in this direction is being carried out in our laboratory.

Conclusion

In summary, we have synthesized a loose-packed nanoflake $Ni(OH)_2$ material using a facile chemical precipitation method and applied its microstructure for an electrochemical capacitor. The XRD, SEM, TEM, and BET specific surface area studies show that the as-prepared $Ni(OH)_2$ materials has a less crystallization, nanoflake structure and a narrow mesoporous distribution at around 4–10 nm. The unique microstructure can accommodate the electroactive species in the solid bulk electrode material. The specific capacitance of the $Ni(OH)_2$ materials at 5, 10, 20, and 30 mA were 2,055, 1,907, 1,645, and 1,486 F/g, which shows a better rate capability and great potential as the electrode materials for electrochemical capacitors. The maximum specific capacitance is the highest reported for a $Ni(OH)_2$ electrode. Even though we do not fully understand the fundamental structure of $Ni(OH)_2$ materials, the strategy reported here should be viable to extend to other transition metal oxides systems.

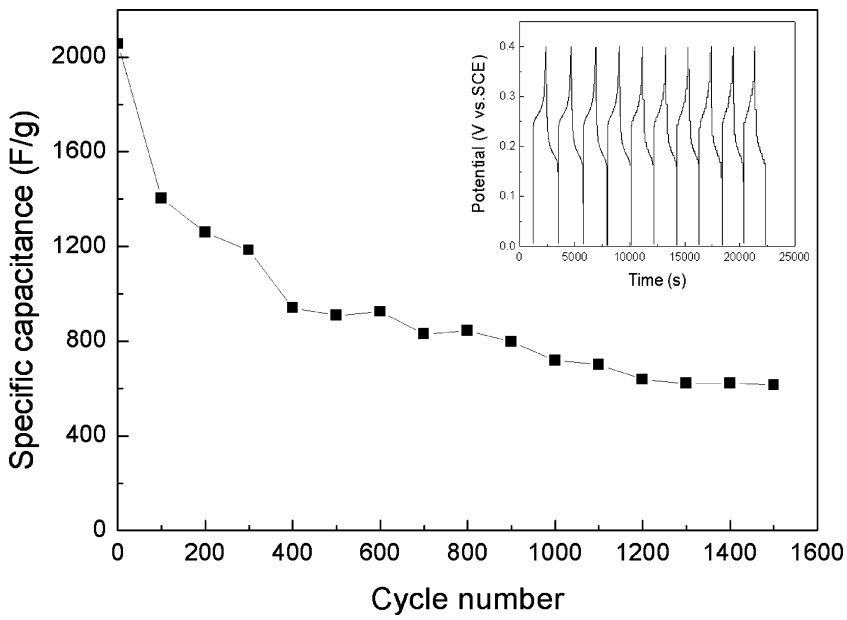

Fig. 9 Cycle life of the as-prepared $Ni(OH)_2$ electrode at the discharge current of 5 mA in 2 M KOH electrolyte. The *inset* is the charge/discharge curves of the $Ni(OH)_2$ electrode

Acknowledgment The authors acknowledge the financial support by the National Natural Science Foundation of China (no. 50602020) and the National Basic Research Program of China (no. 2007CB216408).

References

1. Winter M, Brodd RJ (2004) Chem Rev 104:4245
2. Conway BE (1999) Electrochemical supercapacitors. Scientific fundamentals and technological applications. Plenum, New York
3. Liang YY, Bao SJ, Li HL (2007) J Solid State Electrochem 11:571
4. Wang YG, Li HQ, Xia YY (2006) Adv Mater 18:2619
5. Prasad KR, Miura N (2004) Electrochem Commun 6:1004
6. Pang SC, Anderson MA, Chapman TW (2000) J Electrochem Soc 147:444
7. Tilak BV, Chen CP (1996) J Electrochem Soc 143:3791
8. Lin C, Ritter JA, Popov BN (1998) J Electrochem Soc 145:4097
9. Wu MQ, Gao JH, Zhang SR, Chen A (2006) J Porous Mater 13:407
10. Zhao DD, Bao SJ, Zhou WJ, Li HL (2007) Electrochem Commun 9:869
11. Yang DN, Wang RM, He MS, Zhang J, Liu ZF (2005) J Phys Chem B 109:7654
12. Park JH, Kim S, Park OO, Ko JM (2006) Appl Phys A 82:593
13. Hosono E, Fujihara S, Honma I, Ichihara M, Zhou H (2006) J Power Sources 158:779
14. Christoskova SG, Stoyanova M, Georgieva M, Mehandjiev D (1999) Mater Chem Phys 60:39
15. Cao L, Lu M, Li HL (2005) J Electrochem Soc 152:A871
16. Gupta V, Kusahara T, Toyama H, Gupta S, Miura N (2007) Electrochem Commun 9:2315
17. Broughton JN, Brett MJ (2005) Electrochim Acta 50:4814
18. Djurfors B, Broughton JN, Brett MJ, Ivey DG (2005) Acta Mater 53:957
19. Ma SB, Nam KW, Yoon WS, Yang XQ, Ahn KY, Oh KH, Kim KB (2007) Electrochem Commun 9:2807
20. Wang DB, Song CX, Hu ZS, Fu X (2005) J Phys Chem B 109:1125
21. Song QS, Li YY, Chen SLI (2005) J Appl Electrochem 35:157
22. Wu MS, Hsieh HH (2008) Electrochim Acta 53:3427
23. Srinivasan V, Weidner JW (1997) J Electrochem Soc 144:L210
24. Liu KC, Anderson MA (1996) J Electrochem Soc 143:124
25. Cao L, Kong LB, Liang YY, Li HL (2004) Chem Commun 14:1646
26. Toupin M, Brousse T, Belanger D (2002) Chem Mater 14:3946
27. Xing W, Li F, Yan ZF, Lu GQ (2004) J Power Sources 134:324
28. Jayashree RS, Kamath PV (2001) J Appl Electrochem 31:1315
29. Wang RN, Li QY, Wang ZH, Wei Q, Nie ZR (2008) Chem J Chin Univ 29:18
30. Kötz R, Carlen M (2000) Electrochim Acta 45:2483
31. Zheng JP, Cygan PJ, Jow TR (1995) J Electrochem Soc 142:2699
32. Xu MW, Zhao DD, Bao SJ, Li HL (2007) J Solid State Electrochem 11:1101
33. Zhang SS, Xu K, Jow TR (2004) Electrochim Acta 49:1057
34. Kamath PV, Dixit M, Indira L, Shukla AK, Kumar VG, Munichanduaiah N (1994) J Electrochem Soc 141:2956